



Lithium Lanthanum Titanate derived from Lanthanum Oxalate as the Anode Active Material in Lithium-ion Batteries

Benediktus Ma'dika¹, Retna Deca Pravitasari², Riesma Tasomara², Ade Utami Hapsari², Damisih², Sri Rahayu², Hanif Yuliani², Oka Pradipta Arjasa², Nendar Herdianto², Yelvia Deni², Suyanti³, Anne Zulfia Syahrial¹, Mahendra Rao Somalu⁴, Jarot Raharjo^{2,*}

¹Metallurgical and Materials Engineering, Faculty of Engineering, Universitas Indonesia, Jl. Margonda Raya, Depok, 16424, INDONESIA

²Technology Center for Material, National Research and Innovation Agency (BRIN), Building 224, Puspiptek Area, South Tangerang, Banten, 15314, INDONESIA

³Center for Science and Accelerator Technology, National Research and Innovation Agency (BRIN), Jl. Babarsari Kotak Pos 6601 ykbb, Yogyakarta, 55381, INDONESIA

⁴Fuel Cell Institute, Universiti Kebangsaan Malaysia, 43600, Bangi, Selangor Darul Ehsan, MALAYSIA

*Corresponding author

DOI: <https://doi.org/10.30880/ijie.2022.14.02.018>

Received 8 December 2021; Accepted 20 March 2022; Available online 01 June 2022

Abstract: Lithium-ion battery has been drawing attention from researchers due to its excellent properties in terms of electrochemical and structural stability, low cost, and high safety feature, leading to prospective applications in electric vehicles and other large-scale applications. However, lithium-ion batteries are still in charging time owing to its low conductivity, restricting its wide applications in large-scale applications. In this work, therefore, lithium lanthanum titanate (LLTO) was synthesized derived from lanthanum oxalate, as a lanthanum source, for an anode active material application in the lithium-ion batteries due its high electrochemical conductivity and pseudocapacitive characteristics. To the best of our knowledge, our work is the first one to synthesize LLTO from lanthanum oxalate as the lanthanum source. Commercial lithium carbonate and commercial titanium oxide were used as the lithium and titanium sources, respectively. It was used low cost and simple solid-state reaction process to synthesize this material and performed a two-step calcination process at 800 °C for 8 hours and 1050 °C for 12 hours under ambient atmosphere. The physical characteristics showed that LLTO possesses high purity (98.141%) and micro sized grains with abundant empty spaces between the grains. This, therefore, lead to improve electrochemical performances such as stable discharge capacity at low potential even near to zero (98.67 mAh), and a high conductivity of 2.45×10^{-2} S/cm at room temperature. This LLTO is interesting to be used as the anode active material in low potential lithium-ion battery applications.

Keywords: Anode active material, lanthanum oxalate, lithium-ion battery, solid-state reaction, lithium lanthanum titanate

1. Introduction

Lithium-ion batteries (LIBs) have been researched intensively for applications in transportable devices and large-scale energy storage technologies such as electric vehicles (EVs) and energy grids because of their long lifespan, high

energy capacity, and high voltage [1], [2]. Furthermore, LIBs perform based on the intercalation/deintercalation process, where the lithium-ions are either absorbed from the electrolyte and intercalated into the electrode structure (intercalation process) or forced out from the electrode material (deintercalation process) and driven to the electrolyte, depending on the electrical current flow direction [3]. This working mechanism makes LIBs more structurally and electrochemically stable than other batteries. However, the more pronounced range anxiety and longer charging time of the LIB-powered EVs compared to the petrol-fueled vehicles are often mentioned as one of the main issues impeding the broader adoption of LIB in EVs [4]. This is because EVs commonly operate at low ambient temperature, leading to sluggish intercalation kinetics and diffusion of lithium-ions in the electrolyte and electrode materials [4]. Therefore, LIB still needs some improvements in terms of the fast charging performance to meet their practical applications in EVs and other large-scale applications. Fast charging batteries are achievable if they possess high ionic conductivity and electronic conductivity of active materials [5].

Lithium lanthanum titanate (LLTO), with a chemical formula of $\text{Li}_{3x}\text{La}_{(2/3-x)(1/3-2x)}\text{TiO}_3$ ($0.04 < x < 0.16$) and type of perovskite ABO_3 , has been reported to achieve the highest bulk ionic conductivity ($2.4 \times 10^{-2} \text{ S cm}^{-1}$ at room temperature) among the oxide materials [6]–[8]. The high ionic conductivity originates from the presence of La-poor layers and larger lattice parameters of La ions in the ABO_3 -typed LLTO. La-poor layers (Li-rich layers) are composed of approximately all vacant A-sites of the ABO_3 structures, resulting in a large number of vacant sites at the unoccupied 18d and 6a positions which can facilitate large lithium-ion storage and ease lithium-ion motion throughout the LLTO structure [7]–[9]. Meanwhile, the larger lattice parameters of La ions expand and distort a bottleneck (sized of 1.07 \AA which is lower than that of a lithium-ion of 1.18 \AA), enabling the TiO_6 octahedra to tilt and rotate easily which further lowers the lithium-ion activation energy [7]. It makes the lithium-ion percolations occur without difficulty and generates a higher concentration of vacancy that provides more free space for lithium-ion diffusion and storage. Besides, the instability of LLTO against metallic Li enables a direct reduction of Ti^{4+} to Ti^{3+} , thus drastically increasing its electronic conductivity [6]. Moreover, LLTO undergoes an insulator-to-metal transition at high rates of lithium-ion insertion under 1.5 V versus Li^+/Li , and thus suitable for electrode applications in high-rate LIBs [8]. Therefore, LLTO is a promising candidate active material electrode for fast charging LIBs. Even though being sized on a micrometer scale, LLTO can offer a reasonable compromise between high capacity and high rate attributable to its intercalation pseudocapacitive charge storage behavior that can accommodate rapid charge storage and release processes [8].

However, the application of LLTO is still restricted by structural instability and high resistance at grain boundaries which can disrupt the lithium-ion diffusion pathways within the La-poor layers, hence reducing the electrochemical conductivity of LLTO by 2–3 orders of magnitude [10]. There have been several strategies proposed to diminish the grain boundary problems in LLTO such as: 1) substitution of A-sites with other lanthanide ions and alkaline ions; 2) layer modifications by dopants; 3) high-temperature sintering/calcination; 4) anisotropic orientation control [7].

In this work, LLTO has been synthesized through a simple and low-cost solid-state reaction process and subjected to the calcination step at high temperatures. Here, the local lanthanum source was used for the first time to synthesize LLTO. Commercial Li_2CO_3 and commercial anatase- TiO_2 were used as Li and Ti sources, respectively. The local lanthanum oxalate ($\text{La}_2(\text{C}_2\text{O}_4)_3$) used in this work was synthesized by the Center for Accelerator Science and Technology, BATAN, Indonesia, with a lanthanum content of 95.296 % [11]. It was derived from Indonesia monazite sand. The purpose of research was to investigate whether LLTO could be formed if $\text{La}_2(\text{C}_2\text{O}_4)_3$ was used as the lanthanum source and examine its electrochemical performances for the anode active material of lithium-ion batteries. Synthesized LLTO powders were characterized using XRD, SEM and BET. Lithium-ion half cell was then assembled and several electrochemical performance tests were performed including cyclic voltammetry, charging/discharging and electrochemical impedance spectroscopy.

2. Experimental Method

In this method, commercial anatase- TiO_2 (Sigma Aldrich, Germany), commercial Li_2CO_3 (Sigma Aldrich, Germany), and local $\text{La}_2(\text{C}_2\text{O}_4)_3$ were used to synthesize LLTO ($\text{Li}_{0.5}\text{La}_{0.5}\text{TiO}_3$) with moles of 0.05924, 0.0481, and 0.01481 (plus 20% for compensating the evaporated lithium at the high calcination temperature), respectively. The precursors were mixed in ethanol and then milled in a vibrating ball mill at 1200 rpm for 4 hours. The result was dried in a vacuum oven at $120 \text{ }^\circ\text{C}$ for 12 hours. The next step was two-step calcination, where the first step and the second step were performed at $800 \text{ }^\circ\text{C}$ for 8 hours and $1150 \text{ }^\circ\text{C}$ for 12 hours, correspondingly under ambient atmosphere.

The physical characteristics of the LLTO were investigated using several characterization methods. X-ray diffraction (XRD) was used to identify the phases present which was further analyzed using Rietveld Refinement in General Structural Analysis (GSAS). Scanning Electron Microscopy (SEM) was used to investigate the LLTO particles, while Brunauer-Emmett-Teller (BET) isothermal adsorption/desorption was performed at liquid nitrogen (77.3K) temperature to determine LLTO specific surface area and porosity. Grain size distribution was analyzed from SEM image with Origin software. It was previously measured with ImageJ software.

To explore the electrochemical performances, the synthesized LLTO as the active anode material, PVDF (Xiamen Tob New Energy Technology, China) as the binder, and Super P (Xiamen Tob New Energy Technology, China) as the conductive additive were mixed in NMP solution (Xiamen Tob New Energy Technology, China) with the weight ratio of 80%: 10%: 10%, respectively. The slurry obtained from this step was coated onto the copper foil (Xiamen Tob New

Energy Technology, China) as the current collector where the coating thickness was set at 75 μm . And then, it was dried in a vacuum oven at 80 $^{\circ}\text{C}$ for 4 hours. The anode was cut into a size according to the R2032 cell. The lithium-ion half cell was assembled in an Ar gas-filled glove box using LiPF_6 as the electrolyte, the mixture of dimethyl carbonate and ethyl carbonate (1:1) as the solvent, polypropylene as the separator, and lithium foil as the opposing electrode.

The electrochemical performances were measured using several tests. Cyclic voltammetry (CV) was performed at a rate of 120 $\mu\text{V/s}$ in the potential range of 0.6-2.5 V to investigate the lithiation and de-lithiation process. A charging/discharging (CD) test was carried out at a C-rate of 0.5 C in the potential range of 0-2.5 V to determine the capacity. Electrochemical impedance spectroscopy (EIS) characterization was run in a potential static mode with AC impulse voltage of 10 mV RMS in the frequency range of 0.01-20000 Hz to measure the resistance and conductivity.

3. Result and Discussion

3.1 Physical Characteristics of LLTO

XRD characterization of the synthesized LLTO after completing the calcination process at 1500 $^{\circ}\text{C}$ for 12 hours is shown in Fig. 1. In this figure, it can be seen that LLTO was successfully synthesized through solid state method using the local $\text{La}_2(\text{C}_2\text{O}_4)_3$ as the lanthanum source in combination with commercial Li_2CO_3 and commercial anatase- TiO_2 . There are two phases present, namely LLTO with the chemical formula $\text{Li}_{0.5}\text{La}_{0.5}\text{TiO}_3$ (COD 961526421)[12] and $\text{Li}_{1.333}\text{Ti}_{1.667}\text{O}_4$ (COD 961001099) [13]. It has been already confirmed that LLTO could be effectively formed above 1000 $^{\circ}\text{C}$ [7], [14]. Zhan *et al.* (2012) has reported that $\text{La}_2(\text{C}_2\text{O}_4)_3$ experienced thermal decomposition into La_2O_3 and CO_2 in a temperature range of 600-745.6 $^{\circ}\text{C}$ [15], Bat *et al.* (2003) reported that Li_2CO_3 was subjected to thermal decomposition into Li_2O and CO_2 at 772 $^{\circ}\text{C}$ [16]. Finally, TiO_2 , Li_2O , and La_2O_3 reacted with each other through solid-state reaction to form $\text{Li}_{0.5}\text{La}_{0.5}\text{TiO}_3$ [8], [17]. However, Fig. 1 shows that $\text{Li}_{1.333}\text{Ti}_{1.667}\text{O}_4$ is also present, elucidating that LLTO was not completely formed because some fraction of the precursors were transformed into $\text{Li}_{1.333}\text{Ti}_{1.667}\text{O}_4$. This was likely because temperature and time were not optimal for the second stage calcination. Inaguma *et al.*, (1994) observed that lithium oxide could be formed along with LLTO if the calcination process performed outside temperature of 1350 $^{\circ}\text{C}$ and time of 6 h [18]. Because the synthesized LLTO was not completely formed, then, the Rietveld Refinement of General Structural Analysis (GSAS) was performed to determine the weight fraction of each phase. The result showed that $\text{Li}_{0.5}\text{La}_{0.5}\text{TiO}_3$ and $\text{Li}_{1.333}\text{Ti}_{1.667}\text{O}_4$ contents were 98.141 wt% and 1.859 wt%, in turn. This result is in line with the peak intensities shown in Fig. 1 because the peaks of $\text{Li}_{0.5}\text{La}_{0.5}\text{TiO}_3$ are far too high compared to those of $\text{Li}_{1.333}\text{Ti}_{1.667}\text{O}_4$. Thus, it can be concluded that LLTO synthesized from the local $\text{La}_2(\text{C}_2\text{O}_4)_3$ as the lanthanum source is high in purity. Fig. 2 shows the SEM images of LLTO. Fig. 2a is the SEM image with a magnification of 2500X. It can be observed that the LLTO grains were larger and formed into the octahedral morphology. The SEM image in Fig. 2b with a magnification of 5000X displays clearer LLTO grain morphologies in which it can be noticed that there are abundant empty spaces between the grains. The obtained morphology is typical for the LLTO calcined at high temperatures [17], [19].

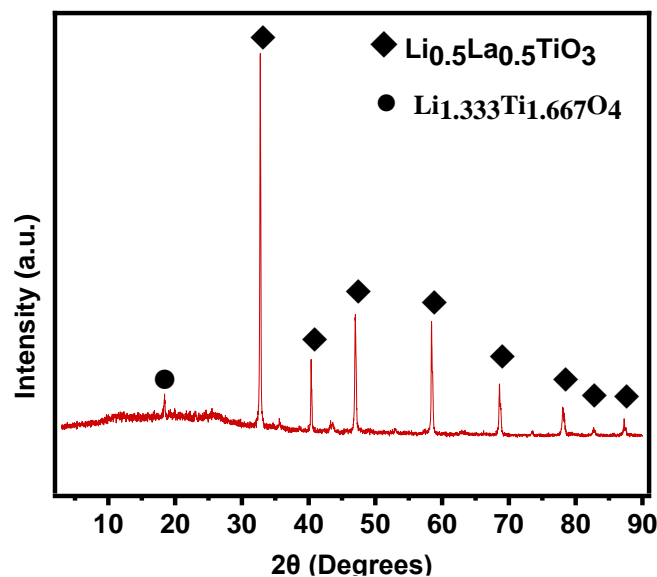


Fig. 1 - XRD pattern of LLTO after calcination at 1500 $^{\circ}\text{C}$ for 12 h under ambient atmosphere

The grain size distribution of LLTO is exhibited in Fig. 2c. It is in the range of 1.5-5.5 μm and the majority of the grains have sizes around 3.0 μm . This grain size range is lower than that of Zhang *et al.* (2020) work, where the LLTO grain size distribution is in the range of 2-20 μm [8]. Still, the grain size distribution is also comparable to that of

Vijayakumar *et al.* (2005) work, where they found the majority of the LLTO grain sizes are ~ 0.2 and $\sim 5 \mu\text{m}$ [17]. The bulk morphology and micron-scaled grain size of LLTO are attributable to the high-temperature calcination process [8]. The isotherm graph of LLTO obtained from the BET method at the liquid nitrogen temperature and relative pressure of 0.00-1.05 is exhibited in Fig. 3. The adsorption and desorption curves are increasing as the relative pressure is increased. This mode corresponds to the type III isotherm without an apparent adsorption/desorption hysteresis, indicating the reversible sorption of LLTO toward N_2 [20]. From BET measurement, the LLTO specific surface area (SSA), the average pore radius, and the total pore volume are found to be $6.666 \text{ m}^2 \text{ g}^{-1}$, 19.671 \AA , and $6.557 \times 10^{-3} \text{ cm}^3 \text{ g}^{-1}$, correspondingly.

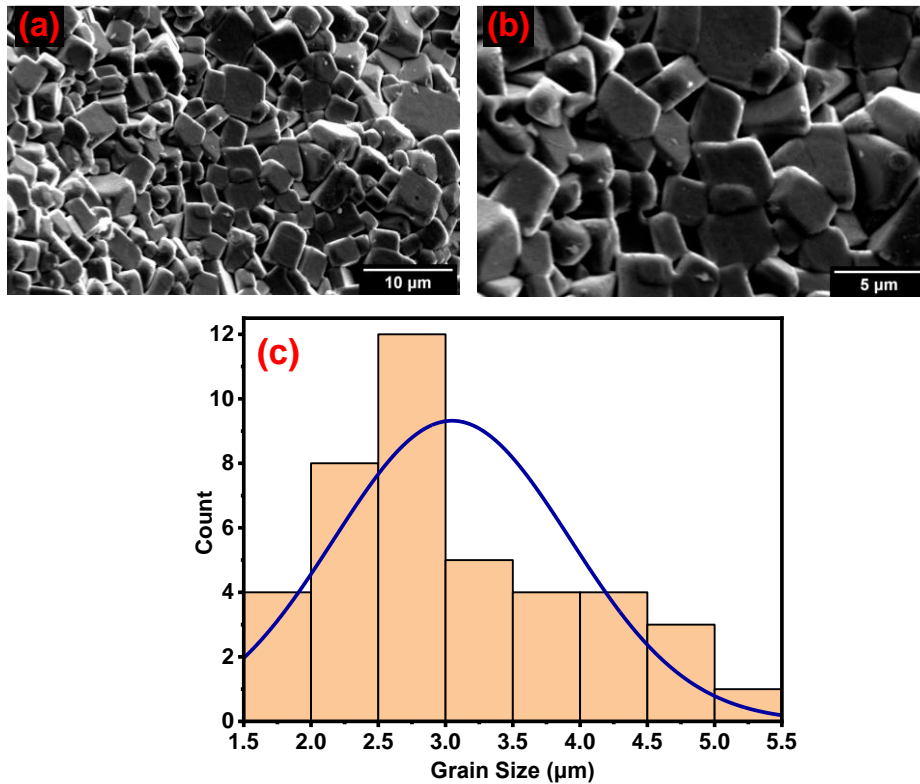


Fig. 2 - SEM images of LLTO with magnifications of (a) 2500X and (b) 5000X; and (c) LLTO grain size distribution

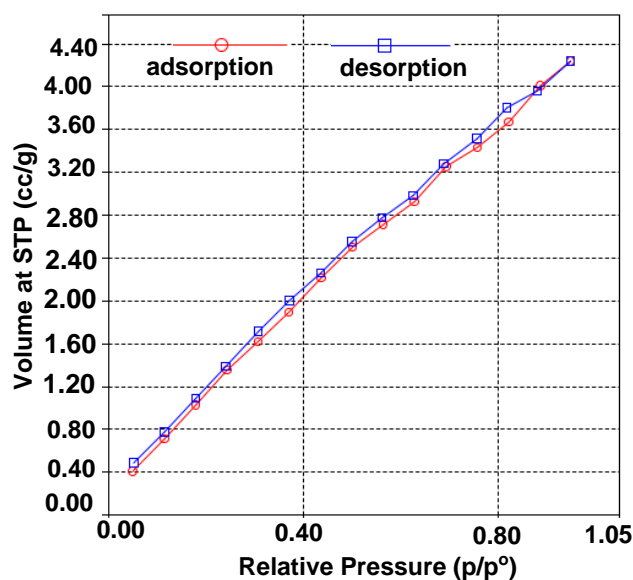


Fig. 3 - Isotherm graph of LLTO obtained from BET method

3.2 Electrochemical Performances of LLTO

A cyclic voltammogram, as shown in Fig. 4 is used to investigate the correlation between the input voltages in the range of 0.6-2.5 V (scan rate of 120 $\mu\text{V/s}$) and output currents. The linear potential scanning was conducted twice when the lithiation and de-lithiation processes. The result curves exhibit wide cathodic and anodic peaks with quasi-rectangular shapes, indicating pseudocapacitance (surface redox reaction) and solid-solution reaction [8], [21]. There are two anodic peaks (1.26 V and 1.68 V) and cathodic peaks (1.04 V and 1.46 V) observed in the figure. The formation of potential peaks during anodic scanning is caused by lithium-ion insertion into the anode structure, while cathodic scanning is caused by the lithium-ion extraction from the anode structure. It is also observed that the lithium-ion can be intercalated into LLTO below the potential of around 1.8 V, while the average value of 1.68V/1.46V indicates the lithium-ion insertion/extraction which is in agreement with the previous work [22]. Still, the average values of the peak couples of 1.26V/1.04V and 1.68V/1.46V correspond to the two-step reduction/oxidation of $\text{Ti}^{4+}/\text{Ti}^{3+}$ in LLTO which is also in agreement with the previous work [21].

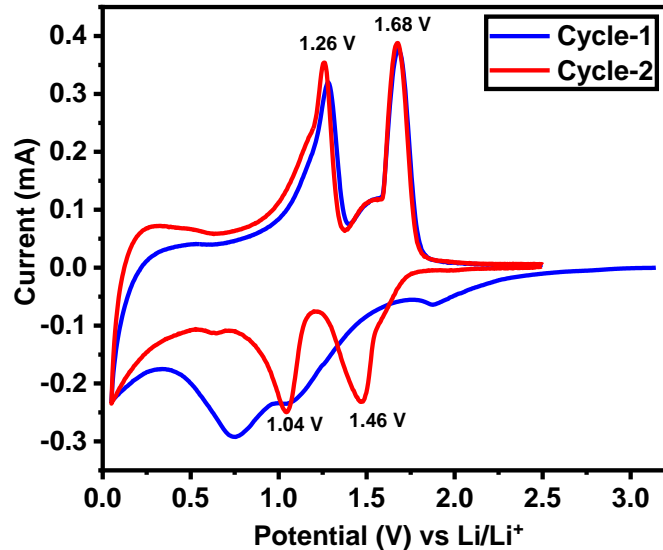


Fig. 4 - Cyclic voltammogram of LLTO

The CV curve shape of the first discharge is dissimilar to that of the second cycle. Furthermore, the reduction peaks shift to higher potentials after the first cycle, signifying that the polarization turn into less significant as a result of improved electrical conductivity of LLTO after lithium-ion insertion [21]. On the other side, the area of the reduction peak below 0.8 V in the first discharge is larger than that in the second cycle. This is caused by the irreversible reaction which might be originated from the electrolyte decomposition [21]. On the other hand, the curve exhibits sharp peaks, indicating good fast charging-discharging characteristics due to the fast diffusion rate of lithium-ions [23]. The cyclic voltammogram of LLTO is certainly influenced by its grain morphologies. It is already known from the previous discussion that LLTO possesses octahedral morphology with empty spaces between its grains. The empty spaces enhance the LLTO specific surface area and thereby further enlarge the contact area between the anode active material, and also the anode active material with the electrolyte solution. This shortens the diffusion length of lithium-ions and enhances the kinetics of the lithiation/de-lithiation process and thus improving fast charging-discharging characteristics [24]. Fig. 5 shows the charge/discharge profile of LLTO which was conducted at a C-rate of 0.5 in the potential range of 0.0-2.5 V. In each cycle, the cell was charged up to a potential of 2.5 V and then discharged down to a potential of 0.0 V. The initial charge and discharge capacities are 85.40 mAh at 2.5 V and 96.24 mAh at 0.050 V, correspondingly, indicating reversible charging/discharging which results in higher discharge capacity than the charge capacity. The initial charge capacity is low due to the presence of electrolyte decomposition at the first charging as confirmed in the above-mentioned CV curve. However, the charge capacities in subsequent cycles are increased, except the fourth cycle experiencing a slight reduction due to the SEI-formation, while the discharging capacities nearly remain the same. This suggests that the effects of the SEI-forming electrolyte decomposition, carbon, and binder have little effects to disturb the charging/discharging reversibility of LLTO for the subsequent cycles [25]. Interestingly, the second, third, and fourth cycles are nearly superimposed with each other, indicating good reversibility of the LLTO during the charging and discharging process. In this condition, the maximum charge and discharge capacities are 93.35 mAh at 2.50 V and 98.67 mAh at 0.050 V, respectively. For comparison, our charging/discharging curve is comparable to that of Zhang *et al.*, (2020) work [8]. They found that LLTO exhibits dual merits, both of higher capacity and lower working potential, and for that reason finding its prospective commercial potential applications.

Fig. 6 exhibits the Nyquist plot of LLTO obtained from the EIS measurement in the potentiostatic mode at the frequency of 0.01-20000 Hz and AC impulse voltage of 10 mV RMS. The curve consists of half a semicircle at the high

to medium frequencies and an upright line at the low frequency. The intercept at the real axis (Z_{re}), semicircle radius, and the slanted line stand for the ohmic resistance (R_s), charge transfer resistance (R_{ct}), and Warburg impedance (Z_w), in turn. This is also confirmed by our fitted equivalent circuit model in the graph which consists of R_s , R_{ct} , constant phase element (CPE), Warburg open (W_o), and Warburg (W). R_s is formed due to the electronic conductivity of the separator, electrolyte, and anodes, while Warburg is stemmed from the diffusion of lithium-ions in the anode active materials [26]. The fitted model shows that the values of R_s and R_{ct} are 3.96Ω and 254.29Ω , respectively. These values were used to calculate the total conductivity of LLTO and it was found to be $2.4 \times 10^{-2} \text{ S cm}^{-1}$ at room temperature. This value is higher than that of previously reported [6], [7]. The enhanced conductivity of the LLTO in our work is primarily caused by two factors. First, the presence of the two-step reduction/oxidation of Ti^{4+}/Ti^{3+} which provides additional electrons and thus drastically increases the electronic conductivity [27]. Second, the presence of the empty spaces can enlarge the contact area between active material grains, and the active material grains with the electrolyte solution, shortening the diffusion length of lithium-ions and enhancing kinetics of lithiation/de-lithiation process, and thereby ameliorating the lithiation and de-lithiation processes and fast charging-discharging behavior [24]. The ionic conductivity obtained from this work compared with other work from literature was shown by Table 1.

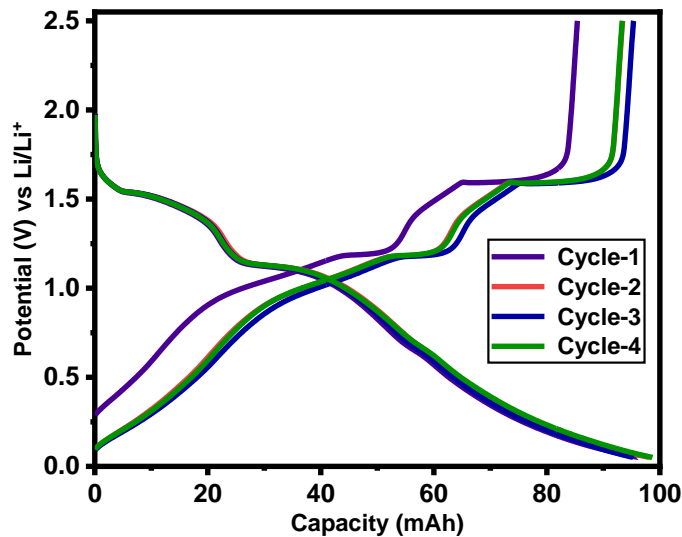


Fig. 5 - Charge/discharge profile of LLTO

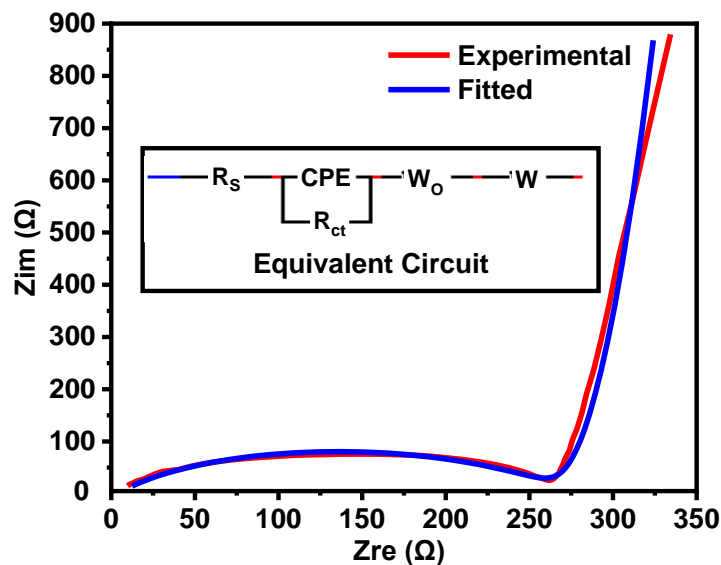


Fig. 6 - Nyquist plot of LLTO

Table 1 - Ionic conductivity obtained from this work compared with literature

Author's work	LLTO composition	Ionic conductivity	Reference
---------------	------------------	--------------------	-----------

(S.cm-1)			
This work	$\text{La}_{0.5}\text{Li}_{0.5}\text{TiO}_3$	2.4×10^{-2}	-
Wang <i>et al.</i>	$\text{Li}_{0.33}\text{La}_{0.57}\text{TiO}$	1.6×10^{-5}	[6]
Sun <i>et al.</i>	$\text{Li}_{3x}\text{La}_{(2/3-x)(1/3-2x)}\text{TiO}_3$ ($0.04 < x < 0.16$)	$\sim 1.53 \times 10^{-3}$	[7]
Symington <i>et al.</i>	$\text{Li}_{0.16}\text{La}_{0.62}\text{TiO}_3$	0.68×10^{-4}	[10]
Ibarra <i>et al.</i>	$\text{Li}_{3x}\text{La}_{(2/3-x)(1/3-2x)}\text{TiO}_3$ ($0.03 < x < 0.167$)	$4 \times 10^{-4} \sim 1 \times 10^{-3}$	[12]
Stamare <i>et al.</i>	$\text{Li}_{3x}\text{La}_{(2/3-x)(1/3-2x)}\text{TiO}_3$ ($0.04 < x < 0.16$)	$\sim 1 \times 10^{-3}$	[14]
Bhat <i>et al.</i>	$\text{La}_{0.55}\text{Li}_{0.35}\text{TiO}$	$8.63 \times 10^{-4} \sim 8.95 \times 10^{-4}$	[16]
Inaguma <i>et al.</i>	$\text{La}_{0.5}\text{Li}_{0.5}\text{TiO}_3$	1×10^{-3}	[18]
	$\text{La}_{0.55}\text{Li}_{0.35}\text{TiO}_3$	1×10^{-3}	
	$\text{La}_{0.6}\text{Li}_{0.2}\text{TiO}_3$	6.3×10^{-4}	
	$\text{La}_{0.63}\text{Li}_{0.1}\text{TiO}_3$	7.9×10^{-4}	
Hua <i>et al.</i>	$\text{La}_{0.27}\text{Li}_{0.54}\text{TiO}_{2.945}$	3.9×10^{-3}	[21]
Chen <i>et al.</i>	$\text{La}_{0.55}\text{Li}_{0.35}\text{TiO}_3$	$0.89 \times 10^{-3} \sim 1.19 \times 10^{-3}$	[22]
	$\text{La}_{0.57}\text{Li}_{0.29}\text{TiO}_3$	$0.66 \times 10^{-3} \sim 1.17 \times 10^{-3}$	
Trong <i>et al.</i>	$\text{Li}_{0.33}\text{La}_{0.57}\text{TiO}$	1.8×10^{-3}	[28]

4. Conclusion

In this work, LLTO ($\text{Li}_{0.5}\text{La}_{0.5}\text{TiO}_3$) was successfully synthesized with a high content (98.141 wt.%) from local $\text{La}_2(\text{C}_2\text{O}_4)_3$ in combination with commercial anatase- TiO_2 and commercial Li_2CO_3 through a solid-state reaction process at high calcinating temperature. The high calcination temperature rendered the LLTO grains to have micro sizes (1.5-5.5 μm) and octahedral shapes with abundant empty spaces between the grains, resulting in a specific surface area of 6.666 $\text{m}^2 \text{g}^{-1}$. This leads to improve electrochemical performances. Functioning as the LIB anode active material, LLTO exhibits pseudocapacitance (surface redox reaction) and solid-solution reaction. These characteristics have been confirmed by other work to give a reasonable compromise between high capacity and high rate. Furthermore, the LLTO also could maintain high and stable discharge capacity at low potential even near to zero (98.67 mAh at 0.050 V). In terms of conductivity, the LLTO has a larger value ($2.4 \times 10^{-2} \text{ S cm}^{-1}$) at room temperature compared to that previously reported. Therefore, the synthesized LLTO in this work is favorable for anode active material in low potential lithium-ion batteries.

Acknowledgment

The authors would like to express their gratitude for financial and facility supports from Technology Center for Material - National Research and Innovation Agency (BRIN), Indonesia. The author also would like to thank Dr. Eng. Abdulloh Rifai for coin cell battery fabrication and Dr. Achmad Subhan for cyclic voltammetry and charge-discharge analysis.

References

- [1] Lipu MSH, Hannan MA, Hussain A, Hoque MM, Ker PJ, Saad MHM, Ayob A., "A review of the state of health and remaining useful life estimation methods for lithium-ion battery in electric vehicles: Challenges and recommendations," *Journal of Cleaner Production*, vol. 205. Elsevier, pp. 115–133, Dec. 20, 2018.
- [2] M. Wang and Y. Tang, "A Review on the Features and Progress of Dual-Ion Batteries," *Advanced Energy Materials*, vol. 8, no. 19. John Wiley & Sons, Ltd, p. 1703320, Jul. 01, 2018.
- [3] G. L. Plett, *Battery Management Systems: Battery Modelling*, Volume 1. Artec Houses, 2015.
- [4] Tomaszewska A, Chu Z, Feng X, O’Kane S, Liu X, Chen J, Ji C, Endler E, Li R, Liu L, Li Y, Zheng S, Vetterlein S, Gao M, Du J, Parkes M, Ouyang M, Marinescu M, Offer G, Wu B., "Lithium-ion battery fast charging: A review," *eTransportation*, vol. 1. Elsevier B.V., p. 100011, Aug. 01, 2019.
- [5] Zhu GL, Zhao CZ, Huang JQ, He C, Zhang J, Chen S, Xu L, Yuan H, Zhang Q., "Fast Charging Lithium Batteries: Recent Progress and Future Prospects," *Small*, vol. 15, no. 15. John Wiley & Sons, Ltd, p. 1805389, Apr. 01, 2019.
- [6] M. J. Wang, J. B. Wolfenstine, and J. Sakamoto, "Mixed Electronic and Ionic Conduction Properties of Lithium Lanthanum Titanate," *Advanced Functional Materials*, vol. 30, no. 10, p. 1909140, Mar. 2020.
- [7] Y. Sun, P. Guan, Y. Liu, H. Xu, S. Li, and D. Chu, "Recent Progress in Lithium Lanthanum Titanate Electrolyte

- towards All-Solid-State Lithium Ion Secondary Battery,” *Critical Reviews in Solid State and Materials Sciences*, vol. 44, no. 4. Taylor and Francis Inc., pp. 265–282, Jul. 04, 2019.
- [8] Zhang L, Zhang X, Tian G, Zhang Q, Knapp M, Ehrenberg H, Chen G, Shen Z, Yang G, Gu L, Du F., “Lithium lanthanum titanate perovskite as an anode for lithium-ion batteries,” *Nature Communications*, vol. 11, no. 1, pp. 1–8, Dec. 2020.
- [9] S. L. Fernandes, G. Gasparotto, G. F. Teixeira, M. A. Cebim, E. Longo, and M. A. Zaghete, “Lithium Lanthanum Titanates,” *Ceramics International*, vol. 44, no. 17, pp. 21578–21584, Dec. 2018.
- [10] Symington AR, Molinari M, Dawson JA, Statham JM, Purton J, Canepa P, Parker SC., “Elucidating the nature of grain boundary resistance in lithium lanthanum titanate,” *Journal of Materials Chemistry A*, vol. 9, no. 10, pp. 6487–6498, Mar. 2021.
- [11] M. V Purwani, S. Suyanti, and W. A. Adi, “Thermal Decomposition Kinetics of Lanthanum Oxalate Hydrate Product Treatment From Monazite,” *Jurnal Sains Materi Indonesia*, vol. 20, no. 2, p. 50, 2019.
- [12] J. Ibarra, A. Várez, C. León, J. Santamaría, L. M. Torres-Martínez, and J. Sanz, “Influence of composition on the structure and conductivity of the fast ionic conductors $\text{La}_{2/3-x}\text{Li}_{3x}\text{TiO}_3$ ($0.03 \leq x \leq 0.167$),” *Solid State Ionics*, vol. 134, no. 3–4, pp. 219–228, 2000.
- [13] A. Deschanvres, B. Raveau, and Z. Sekkal, “Mise en évidence et étude cristallographique d’une nouvelle solution solide de type spinelle $\text{Li}_{1+x}\text{Ti}_{2-x}\text{O}_4$ $0 \leq x \leq 0,333$,” *Materials Research Bulletin*, vol. 6, no. 8, pp. 699–704, 1971.
- [14] S. Stramare, V. Thangadurai, and W. Weppner, “Lithium Lanthanum Titanates: A Review,” *Chemistry of Materials*, vol. 15, no. 21. American Chemical Society, pp. 3974–3990, Oct. 21, 2003.
- [15] G. Zhan, J. X. Yu, Z. G. Xu, F. Zhou, and R. A. Chi, “Kinetics of thermal decomposition of lanthanum oxalate hydrate,” *Transactions of Nonferrous Metals Society of China (English Edition)*, vol. 22, no. 4, pp. 925–934, 2012.
- [16] M. H. Bhat, A. Miura, P. Vinatier, A. Levasseur, and K. J. Rao, “Microwave synthesis of lithium lanthanum titanate,” *Solid State Communications*, vol. 125, no. 10, pp. 557–562, Mar. 2003.
- [17] M. Vijayakumar, Q. N. Pham, and C. Bohnke, “Lithium lanthanum titanate ceramic as sensitive material for pH sensor: Influence of synthesis methods and powder grains size,” *Journal of the European Ceramic Society*, vol. 25, no. 12 SPEC. ISS., pp. 2973–2976, Jan. 2005.
- [18] Y. Inaguma, L. Chen, M. Itoh, and T. Nakamura, “Candidate compounds with perovskite structure for high lithium ionic conductivity,” *Solid State Ionics*, vol. 70–71, no. PART 1, pp. 196–202, 1994.
- [19] D. L. Lu, G. Z. Dai, Y. B. Yao, T. Tao, B. Liang, and S. G. Lu, “Influence of Calcining Temperature on the Property of $\text{Li}_{0.33}\text{La}_{0.56}\text{TiO}_3$ Solid-state Ionic Capacitor,” *Wuji Cailiao Xuebao/Journal of Inorganic Materials*, vol. 33, no. 10, pp. 1077–1082, 2018.
- [20] R. M. Omer, E. T. B. Al-Tikrity, G. A. El-Hiti, M. F. Alotibi, D. S. Ahmed, and E. Yousif, “Porous Aromatic Melamine Schiff Bases as Highly Efficient Media for Carbon Dioxide Storage,” *Processes 2020, Vol. 8, Page 17*, vol. 8, no. 1, p. 17, Dec. 2019.
- [21] C. Hua, X. Fang, Z. Wang, and L. Chen, “Lithium storage in perovskite lithium lanthanum titanate,” *Electrochemistry Communications*, vol. 32, pp. 5–8, 2013.
- [22] C. H. Chen and K. Amine, “Ionic conductivity, lithium insertion and extraction of lanthanum lithium titanate,” *Solid State Ionics*, vol. 144, no. 1–2, pp. 51–57, 2001.
- [23] A. Subhan, F. Oemry, S. N. Khusna, and E. Hastuti, “Effects of activated carbon treatment on $\text{Li}_4\text{Ti}_5\text{O}_{12}$ anode material synthesis for lithium-ion batteries,” *Ionics 2018 25:3*, vol. 25, no. 3, pp. 1025–1034, Jun. 2018.
- [24] Kim T, Choi W, Shin HC, Choi JY, Kim JM, Park MS, Yoon WS., “Applications of voltammetry in lithium-ion battery research,” *Journal of Electrochemical Science and Technology*, vol. 11, no. 1. Korean Electrochemical Society, pp. 14–25, Feb. 01, 2020.
- [25] P.-K. Lee, Y. Li, and D. Y. W. Yu, “Insights from Studying the Origins of Reversible and Irreversible Capacities on Silicon Electrodes,” *Journal of The Electrochemical Society*, vol. 164, no. 1, pp. A6206–A6212, 2017.
- [26] Ding, H. Liu, X. Zhao, L. Pang, L. Deng, and M. Li, “Composite with TiO_2 and extension of discharge voltage range for capacity enhancement of a $\text{Li}_4\text{Ti}_5\text{O}_{12}$ battery,” *RSC Advances*, vol. 7, no. 69, pp. 43894–43904, Sep. 2017.
- [27] S. I. Furusawa, H. Tabuchi, T. Sugiyama, S. Tao, and J. T. S. Irvine, “Ionic conductivity of amorphous lithium lanthanum titanate thin film,” *Solid State Ionics*, vol. 176, no. 5–6, pp. 553–558, Feb. 2005.
- [28] L.D. Trong, T.T. Thao, and N.N. Dinh, “Characterization of the Li-ionic conductivity of $\text{La}_{(2/3-x)}\text{Li}_{3x}\text{TiO}_3$ ceramics used for all-solid state batteries,” *Solid State Ionics*, vol. 278, pp. 228–232, Oct. 2015.